Excitation Energies of Localized Correlated Defects via Quantum Monte Carlo: A Case Study of Mn^{4+}-doped Phosphors

Kayahan Saritas,* Wenmei Ming, Mao-Hua Du, and Fernando A. Reboredo*

Materials Science and Technology Division, Oak Ridge National Laboratory, Oak Ridge, Tennessee 37831, USA

E-mail: saritask@ornl.gov; reboredo@ornl.gov

Abstract

Accurate excitation energies of localized defects have been a long-standing problem for electronic structure calculation methods. Using Mn^{4+}-doped solids as our proof of principle, we show that diffusion quantum Monte Carlo (DMC) is able to predict phosphorescence emission energies within statistical error. To demonstrate the generality of our DMC approach for other possible localized defects, we conduct charge density analyses using DMC and density functional theory (DFT). We also identify a new material with an emission energy of 1.97(8) eV, which is close to the optimum of 2.03 eV for a red-emitting phosphor. To our knowledge, our work is the first report on studying excitation energies of a transition metal impurity using an ab-initio many-body electronic structure method. In contrast, semi-local and hybrid-DFT largely underestimates, and fails to reproduce, some of the trends in the emission energies. Our work underscores the importance of an accurate account of exchange, correlation, and excitonic effects for localized excitations in defective solids.

Graphical TOC Entry

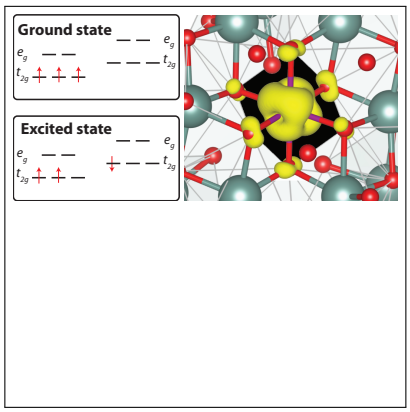

Defects, dopants, and interfaces dominate the spectroscopic properties of insulators and semiconductors. Multivalent ionic defects, for example, can be used as activators within wide-gap materials, inserting multiple electronic states in the band gap.[1,2] These localized electronic states can trap electrons and holes, leading to radiative recombination. Examples of these materials are used in a wide range of applications, such as lighting,[3–6] nuclear detection,[7,8] and lasers.[9] Multivalent dopants that can act as luminescent centers are often rare-earth metals such as Eu^{2+}, Ce^{3+}, and Nd^{3+}.[10–15] However, it is of interest to the scientific community to replace rare-earth metals with lower-cost alternatives, such as transition metals.[16–24] Europium^{3+}-doped Y_2O_3 (Y_2O_3:Eu^{3+}) is the most commonly used red-emitting phosphor in white-light–emitting diodes, thanks to its emission wavelength (energy) of 611 nm (2.03 eV).[23] However, the emission wavelengths of Mn^{4+}-doped hosts are all longer than the Y_2O_3:Eu^{3+} emission wavelength;[23] the shortest are 617 nm in the Na_2SiF_6 host,[21] and 648 nm in an oxide host.[24] Despite their favorable emission wavelengths, fluoride hosts are not suitable for use in fluorescent lamps because of their reactivity with the mercury vapor. For an efficient red phosphor, proximity to the optimum emission energy is critical, because the chromatic response in the human eye decays rapidly away from the optimum.[25]

Theoretical progress in the accurate prediction of optical properties of solids is still mostly limited to crystals and simple defects. Experimental emission energies of doped insulators/semiconductors can be obtained using photoluminescence spectroscopy.[26] Probing local magnetism with atomic precision is also possible.[27] In contrast, most ab-initio electronic structure methods achieve only qualitative agreement on the optical properties of defects and interfaces. Therefore, theoretical methods can only attempt to explain the experimental results, rather than leading materials discovery. Density functional theory (DFT) and related methods[28–30] with empirical corrections to the band gap error are rather common in the literature. However, DFT is a ground-state single-particle theory, which is, in principle, incapable of calculating the transition energy between multi-electron states. In comparison, the *GW* approximation[31,32] is a higher-level theory that explicitly describes the charged excitations. For neutral excitations, the *GW* approach is followed by the Bethe-Salpeter equation (GW-BSE).[33–36] *GW* has been successfully applied to the excited-state properties of pristine materials[37–41] and vacancy defects, including strongly correlated systems.[42–56] For Mott insulators, however, the *GW* method presents some limitations, since the results may strongly depend on the quality of the starting orbitals.[57–59] Compared with the number of studies with pristine solids and vacancy defects, *GW* studies with a transition metal impurity inside an insulating host are very few.[60,61] An alternative many-body method with computational scalability and rigorous treatment of the electron correlation is needed to achieve an accurate prediction of the excited-state properties of imperfect crystalline solids.

In this work, we calculated the optical transition energies of transition metal dopants, using a fundamentally different approach: diffusion quantum Monte Carlo (DMC). DMC is a wavefunction-based method that can capture exchange, correlation, and excitonic effects with high accuracy and no adjustable parameters.[62–64] DMC has been shown to yield very accurate ground- and excited-state properties for challenging problems in DFT, such as fundamental and optical gaps of covalent solids[65–68] and transition metal oxides,[69–75] as well as defect formation[66,69,71,76–79] and cohesive energies.[80–84] To our knowledge, this is the first attempt to calculate the optical transition energies of transition metal dopants using a beyond-DFT method. For finite systems, DMC accuracy is comparable to that of CCSD(T)[85,86] using a quadruple zeta set.[87] However, DMC has cubic scaling (or better, if localized orbitals are used[88–90]) with respect to the number of electrons.[62] To demonstrate our proof of concept, we studied the excited-state properties of Mn^{4+}-doped Al_2O_3, MgO, Y_2O_3, and K_2SiF_6.

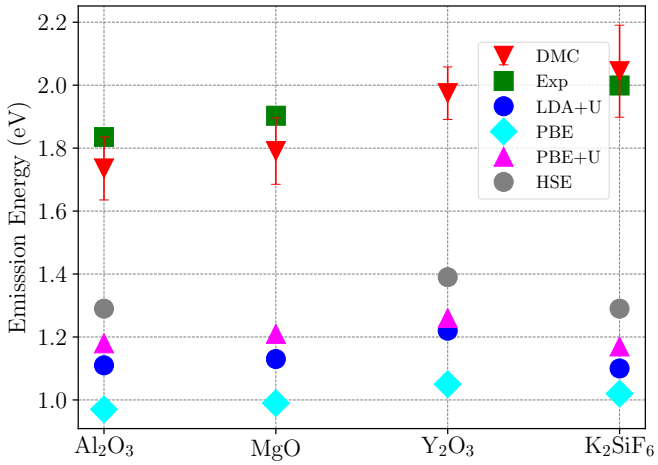

Figure 1: Experimental, DFT-PBE, DFT-HSE, and DMC values of Mn^{4+} emission energies for Al_2O_3, K_2SiF_6, MgO, and Y_2O_3. HSE and PBE results are taken from ref. 91. A U value of 3.9 eV is applied on the d-shells of Mn^{4+} atoms in LDA+U and PBE+U calculations.

.

We showed that our approach is applicable to similar systems, provided that the excitation is sufficiently localized. Unlike the benchmarked DFT calculations, DMC showed excellent agreement with the available experimental emission energies. DMC predicted the emission energy of Mn^{4+}-doped Y_2O_3 to be 1.97(8) eV, which is promising in achieving the desired emission wavelength of 2.03 eV.[25] We show that for the excited-state properties in which we are interested, DMC is capable of achieving near chemical accuracy (0.1 eV/formula unit) in condensed matter systems.

DMC is expected to evolve toward the ground state. Therefore, it may appear that the DMC method alone is not ideal for studying excited-state properties. However, fixed-node DMC (FN-DMC) projects out to the lowest energy eigenstate that is compatible with the symmetry imposed by the trial wavefunction. Therefore, excitation energies can be calculated as the differences between the ground-state energies of different symmetries. If the exact nodal surface is provided in the calculation, then exact ground-state energy is obtained from the FN-DMC method. Nodal errors, however, may be different for different symmetries. For the

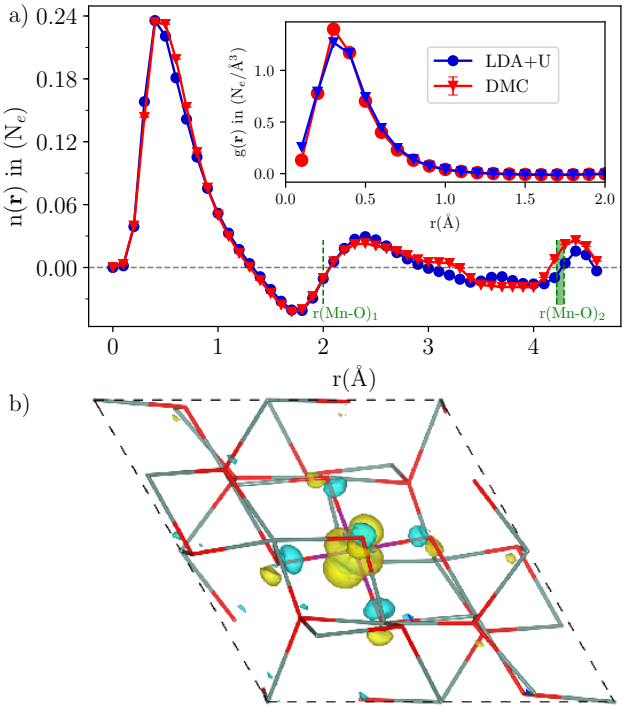

Figure 2: (a) Radial density of the empty Mn-$t_{2g}^{\uparrow}$ orbital as a function of the distance from the Mn atom. r(Mn-O)$_n$ stands for the nth O nearest neighbors of Mn. Inset: Radial distribution function of the same orbital as a function of the distance from the Mn atom. (b) Charge density profile of the empty Mn-$t_{2g}^{\uparrow}$ orbital. The isosurface level is 2% of the maximum value. Yellow and cyan isosurfaces indicate positive and negative values, respectively; whereas red, green, and purple colors indicate Y, O and Mn atoms, respectively.

excited states, it has been shown that DMC energies are accurate if the nodal surface of the excited state cannot be reduced to that of the ground state.[92] In this manuscript, we studied well localized spin-flip transitions at the ground states of the two different spin states. Nevertheless, DMC has been successfully applied to band gaps and quasiparticle gaps of solids[65,70,74,93? –95] and clusters.[96–98]

In our calculations, Mn^{4+} impurities had the d^3 configuration and they were found on the octahedral sites. Therefore, the crystal field created large splitting between the t_{2g} and e_g orbitals. In the ground state, $^4A_{2g}$, three majority-spin electrons were stabilized in

the $t_{2g}^{\uparrow}$ orbitals. The emission spectrum of Mn^{4+} typically showed a sharp line corresponding to the spin- and parity-forbidden excited-state to ground-state, $^2E_g \rightarrow {}^4A_{2g}$, transition.[23] Therefore, the excited state, ^2E_g, had two $t_{2g}^{\uparrow}$ and one $t_{2g}^{\downarrow}$ electrons. Using electronic structure calculation methods, the emission energy was calculated as $E_{em} = E(^2E_g) - E(^4A_{2g})$, where $E(^4A_{2g})$ and $E(^2E_g)$ are the ground- and excited-state total energies. The two states required to calculate the emission energies had different total spins and thus had different symmetries for rotations. The nodal surfaces of the two systems with different total spins had different dimensions for the spin-up and spin-down components of the wave function. Since the spin cannot change in DMC within the standard importance sampling approach, the emission energy is expected to be accurately defined, except for nodal errors and other Hamiltonian errors (Supporting Information).

DFT, DMC, and experimental emission energies of Mn^{4+}-doped hosts are shown in Fig. 1 and some of the numerical values are summarized in Table 1.[99–101] The only exception is the experimental emission energy of the Y_2O_3:Mn^{4+} structure, as it is not available to our knowledge. DMC emission energies were in very good agreement with the experiments: experimental emission energies were found almost within the 1-σ uncertainty of the DMC energies. In contrast, Perdew-Burke-Ernzerhof (PBE)[102] underestimated the emission energies by around 0.8–0.9 eV on average, while for Heyd-Scuseria-Ernzerhof (HSE), the average underestimation was around 0.6–0.7 eV. Figure 1 shows that localized density approximation (LDA)+U and PBE+U follow the same trend as in HSE, although with a larger underestimation. The +U method can help DFT capture some of the static correlation effects, as in Mott insulators, which descend from the multideterminant nature of the electronic wave function.[103] Compared with PBE and PBE+U, the relative success of HSE in predicting the emission energies may point to a deficiency in the exchange or dynamical correlation of the DFT functionals. HSE includes a larger portion of exact exchange

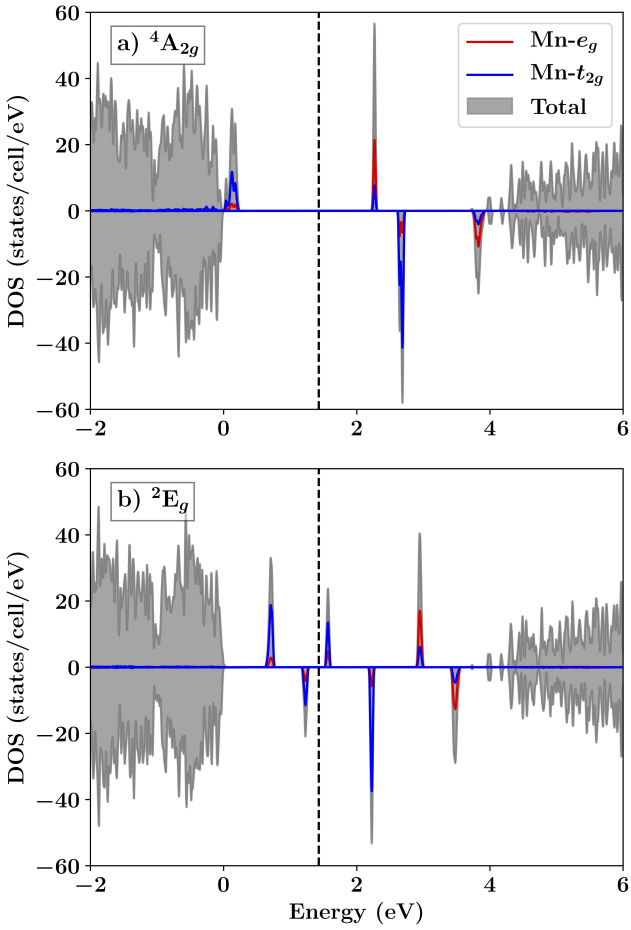

Figure 3: Density of states (DOS) for Mn^{4+} doped Y_2O_3 calculated using the DFT-local density approximation method. DOS is projected onto the e_g and t_{2g} orbitals of Mn^{4+}. The $^4A_{2g}$ ground state is given in (a) and the ^2E_g excited state in (b). The dashed line is plotted to distinguish occupied and unoccupied states.

compared with PBE while having the same correlation functional. It can be expected that, by tuning the amount of exact exchange, HSE can be made to yield more accurate emission energies. However, tuning does not guarantee that HSE can predict the accurate emission energy trends between different families of host materials (e.g., oxides vs. fluorides). Coordination and chemistry-specific tuning in hybrid-DFT can be performed, although at a significant loss for the ab-initio character of the calculations. Table 1 shows that HSE functionals with exact exchange ratios of 0.2–0.4 yield very accurate band gaps for the pristine crystals of the hosts studied in this work. Therefore, fur-

ther tuning of the exact exchange for more accurate emission energies can potentially yield inaccurate band gaps for the pristine host materials. In this respect, the accurate electron correlation through DMC appears to be critical to obtaining the correct emission energy trends across different host structures.

To demonstrate the generality of our approach to the excited-state properties of any localized defect, we studied the localized nature of our proof-of-concept $^4A_{2g} \rightarrow ^2E_g$ transition in Mn^{4+} defects. Figure 2a shows the radial density centered around the Mn^{4+} atom, $n(\mathbf{r})$, for the empty $t_{2g}^{\uparrow}$ orbital in the ^2E_g state. $n(\mathbf{r})$ was obtained simply by subtracting the majority-spin excited state charge density, $\rho_x^{\uparrow}$, from the majority-spin ground-state charge density, $\rho_g^{\uparrow}$. Therefore, $n(\mathbf{r})$ is defined as $\rho_g^{\uparrow} - \rho_x^{\uparrow}$. A similar analysis is also possible where $n(\mathbf{r}) = \rho_x^{\downarrow} - \rho_g^{\downarrow}$ (see Supporting Information). We found that $n(\mathbf{r})$ in Fig. 2a provided richer information regarding the difference between DMC and DFT results. In comparison, the change in total spin polarization in both LDA+U and DMC, $(\rho_x^{\uparrow} - \rho_x^{\downarrow}) - (\rho_g^{\uparrow} - \rho_g^{\downarrow})$, quickly went to zero beyond the first-nearest oxygen neighbors of Mn^{4+} (see Supporting Information). The inset of Fig. 2a shows the radial distribution function, $g(\mathbf{r})$, of the same radial density. $n(\mathbf{r})$ is also radially more sensitive than $g(\mathbf{r})$ in the tails of a distribution. Therefore, $n(\mathbf{r})$ more strongly magnifies the differences between DMC and LDA+U densities. It can be seen that $g(\mathbf{r})$ quickly decays to zero near 1 Å for both LDA+U and DMC densities. Nevertheless, the $n(\mathbf{r})$ from both LDA+U and DMC are indeed very similar to each other with a cosine similarity of 99%. Both DMC and LDA+U $n(\mathbf{r})$ have two distinguishable fluctuations that coincide with the first- and second-nearest oxygen neighbor distances of the centered Mn^{4+} atom shown in Fig. 2b. These fluctuations correspond to the change in the majority-spin distribution around the oxygen atoms, in response to the excitation from the $^4A_{2g}$ to the ^2E_g state. It can be seen that the amplitude of the second fluctuation is smaller than that of the first one. The Mn^{4+} has 6 first-nearest oxygen neighbors at a radius of nearly 2.00 Å, while it has 12 second-nearest oxygen neighbors at a radius between 4.22 and 4.29 Å. Thus, the change of polarization on an individual second-nearest-neighbor oxygen atom must be even smaller. Note that substantial differences between the DFT and DMC excitation energies remained, despite the large similarities in the spin densities, underscoring the difficulties that need to be overcome in DFT.[112]

In spite of its underestimation of the emission energies, the success of DFT can be measured in how well it can reproduce the trends. Therefore, we investigated two main trends in our data: (1) emission energies within oxide hosts and (2) emission energy differences between different family hosts, such as oxides and fluorides. Within the oxide host structures only, going from Al_2O_3 to Y_2O_3 in Fig. 1, the emission energies from PBE, HSE, and DMC all yield increasing trends. It was expected that the emission energies of fluoride host structures would, in general, be larger than those of the oxide host structures.[91,113] To compare the trends between different family hosts, we chose the emission energies of Al_2O_3 and K_2SiF_6 hosts. The experimental emission energies of Al_2O_3 and K_2SiF_6 differed by around 0.17 eV, which was the largest emission energy difference between any structures we studied. PBE and HSE were not able to reproduce this difference. In fact, HSE predicted Al_2O_3 and K_2SiF_6 emission energies as isoenergetic (1.29 eV). In comparison, DMC predicted the emission energy difference as 0.27(18) eV, which was accurate within the error bars.

The success of DFT in predicting the emission energy trends within the same family hosts was also related to the structural parameters and the hybridization strength between the Mn-d and valence O-p orbitals.[23,91] Table 1 shows that average nearest-neighbor Mn-O distances, r_{Mn-O}, increase from 1.91 to 2.00 Å in Al_2O_3, MgO, and Y_2O_3 host structures and are positively correlated to the emission energies. A density-of-states (DOS) analysis from DFT was helpful in understanding the relationships among structural parameters, hybridization strength, and emission energies. Figure 3 shows the DOS obtained using DFT-LDA for

Table 1: Average bond distances in the Mn^{4+} octahedra (in Å); PBE, HSE, and experimental Mn^{4+} emission energies and band gaps (in eV) for the pristine compounds are given.

		Emission energies (eV)			Band gaps (eV)		
	$r_{Mn-\{O,F\}}$ (Å)	PBE[91]	HSE[91]	Exp.	PBE	HSE	Exp.
Al_2O_3	1.905	0.97	1.29	1.835[99]	6.05[104]	9.2[105]	8.7[106]
MgO	1.958	0.99	-	1.903[101]	5[107]	7.57[107]	7.8[107]
Y_2O_3	2.003	1.05	1.39	-	4.27[108]	5.68[108]	5.6[109]
K_2SiF_6	1.830	1.02	1.29	1.999[100]	8.16[110]	-	5.6[111]

the ground and excited states of the Mn^{4+}-doped Y_2O_3 as an example of the nature of the excitation. The $^4A_{2g}$ ground state underwent a small Jahn-Teller distortion, which was strongly hybridized with the valence band that was dominated by O-p states (see Supporting Information). The Mn^{4+} emission ($^2E_g \rightarrow {}^4A_{2g}$) involved a spin flip of an electron from minority to majority spin t_{2g} orbitals. Therefore, the emission energy was nearly independent of the crystal field splitting and the hybridization on the e_g orbitals. The average positions of the t_{2g} and e_g states did not change with the Mn^{4+} emission. However, in ^2E_g, empty t_{2g} states were closer to the valence band compared with the t_{2g} states of $^4A_{2g}$. Since the hybridization occurred between the empty metal orbitals and O-p states, hybridization decreased the total energy of ^2E_g more strongly. Therefore, increased hybridization should have led to lower ^2E_g energies and decreased emission energy.

When emission energies between different families are compared, the rationale from the bond distances and hybridization strengths may not hold. In oxide hosts, increased bond distances lead to a smaller hybridization between the Mn d and O p shells. However, when a fluoride host structure is compared with that of the oxide hosts, the emission energies cannot be deduced based solely on the bond distances. Fluorine has larger electronegativity than oxygen. Therefore, r_{Mn-F} is expected to be smaller than r_{Mn-O}, under otherwise similar conditions. Because of their larger electronegativity, fluorine atoms have a weaker hybridization strength with the d-shell of the transition metal impurity. Weaker hybridization means that the excited state of the defect is less stable and therefore has larger emission energies. Across different host materials, the differences in these qualities are not explained accurately using DFT; this lack of accuracy leads to substantial underestimations and inaccurate trends in the emission energies.

In summary, the DMC calculations presented herein have wider implications for studying excited-state properties of crystal imperfections. To our knowledge, our work is the first attempt to study the optical transitions of transition metal oxide defects using a beyond-DFT method. The approach presented is quite general in its application for localized defects. DMC is truly ab-initio, non-perturbative, and many-body in character. In our case, we presented a new material—Mn^{4+}-doped Y_2O_3—with an emission energy of 1.97(8), which is very close to the desired emission energy of 2.03 eV for a red-emitting phosphor for optimal white light light-emitting diode efficiency. The increasing computational resources available, and the recent success of DMC for calculating the ground and excited states of transition metal oxides in the literature, indicate positive outcomes for further applications to the excited-state properties of extended systems.

Geometry optimization and DFT calculations. Optimization of the geometric coordinates using DMC is computationally very demanding. Therefore, we optimized the geometric coordinates of the ground and excited states of all Mn^{4+}-doped materials with the DFT HSE functional[28] using VASP code and projector-augmented wave pseudopotentials.[114–116] A force convergence of 0.05 eV/Å was applied to all atoms. To ensure that there were no variations between the optimized ge-

ometries of different DFT methods, we performed DFT calculations using PBE and HSE functionals while cross-checking the excitation energies and geometries for each method. A U value of 3.9 eV was applied on the *d*-shell of the Mn^{4+} for calculations in Fig. 1. The choice of the DFT method for geometry optimization had almost no influence on the emission energies we calculated (see Supporting Information). For the benchmark LDA+U and PBE+U calculations[29,30] calculations, we used a U value of 3.9 eV on the *d* orbitals of Mn atoms.

DMC calculations. All DMC calculations were performed using QMCPACK,[?] and the calculation workflows were carried out using the NEXUS[117] software suite. The plane-wave DFT QUANTUM ESPRESSO[118] code was used to generate DMC trial-wave functions in a single Slater determinant form. We used an LDA+U method[119,120] to generate the trial wavefunctions, where the repulsion between Mn 3*d* electrons was varied from 0 to 8 eV. The +U method was used only as a variational parameter to optimize the nodal surfaces. Wavefunction optimization using the LDA+U[29,119] trial wavefunctions is given in the Supporting Information. The fixed node, pseudopotential, and localization errors are well-identified Hamiltonian errors. We included up to three-body Jastrow[121] parameters and performed variance and energy minimizations[122] consecutively at the VMC level to optimize the many-body trial wavefunction.

In our DMC calculations, we used norm-conserving pseudopotentials that were optimized within LDA to replace chemically inert core electrons.[64,123,124] In all the DFT calculations, a kinetic energy cutoff of 350 Ry was used to ensure a convergence of 1 meV/atom. The list of pseudopotentials used for each atom is shown in the Supporting Information. All the pseudopotentials used in this work were tested for ground- and excited-state properties using DMC.[64,71,80,80,125–127] Further tests of the accuracy of these pseudopotentials for spin excitations will be published elsewhere. The smallest cell we used was Mn^{4+} doped in Y_2O_3, which contained 40 atoms. The largest cell we used was Mn^{4+}-doped Al_2O_3, which contained 80 atoms. In principle, DMC calculations must be extrapolated to the infinite size limit. However, this extrapolation was avoided in our calculations because of computational limitations. Owing to the localized nature of the excitation within the simulation cell and the use of identical lattice parameters, the energy difference between the excited- and ground-state structures (emission energy) benefited from systematic error cancellation. All DMC calculations were performed using a 2×2×2 reciprocal grid with a target statistical error bar of < 0.1 eV. In our case, this corresponded to approximately a minimum of 5000 statistical DMC steps using 2048 walkers for each structure. We checked the convergence of our results with respect to the time step used and hence used a time step of 0.01 Ha^{-1} in all our calculations.

Charge density analysis. Since density is a quantity that does not commute with the FN-DMC Hamiltonian, the collected DMC density is actually a mixed estimator.[62] To obtain the pure fixed-node density, ρ, two extrapolation formulas can be used: $\rho_1 = 2\rho_{DMC} - \rho_{VMC} + \mathcal{O}[(\Phi - \Psi_T)^2]$ and $\rho_2 = 2\rho^2_{DMC}/\rho_{VMC} + \mathcal{O}[(\Phi - \Psi_T)^2]$.[62] The accuracy of the estimators depends on the quality of the trial wavefunction, $(\Phi - \Psi_T)$, and both interpolation methods should yield almost identical observables when the trial wavefunction is high in quality. We compare both extrapolation schemes in the Supporting Information and show that two methods yield the same density to a large degree. Therefore, we report the extrapolated densities using ρ_1.

This manuscript has been authored by UT-Battelle, LLC under Contract No. DE-AC05-00OR22725 with the US Department of Energy (DOE). The US government retains and the publisher, by accepting the article for publication, acknowledges that the United States Government retains a nonexclusive, paid-up, irrevocable, worldwide license to publish or reproduce the published form of this manuscript, or allow others to do so, for US government purposes. DOE will provide public access to these results of federally sponsored research in accordance with the DOE Public

Access Plan (http://energy.gov/downloads/doe-public-access-plan)

Supporting Information Available

An overview of the DMC method and the approximations involved, the DMC time step and wavefunction optimization tests, the library of the pseudopotentials used, and additional charge density analysis of DFT and DMC calculations is provided as a text document.

References

(1) Biswas, K.; Du, M.-H. Energy Transport and Scintillation of Cerium-Doped Elpasolite Cs_2LiYCl_6: Hybrid Density Functional Calculations. *Phys. Rev. B* **2012**, *86*, 014102.

(2) Du, M.-H. Using DFT Methods to Study Activators in Optical Materials. *ECS J. Solid State Sci.Tech.* **2016**, *5*, R3007–R3018.

(3) Setlur, A. A.; Radkov, E. V.; Henderson, C. S.; Her, J.-H.; Srivastava, A. M.; Karkada, N.; Kishore, M. S.; Kumar, N. P.; Aesram, D.; Deshpande, A. et al. Energy-Efficient, High-Color-Rendering LED Lamps Using Oxyfluoride and Fluoride Phosphors. *Chem. of Mater.* **2010**, *22*, 4076–4082.

(4) Meyer, J.; Tappe, F. Photoluminescent Materials for Solid State Lighting: State of the Art and Future Challenges. *Advanced Opt. Mater.* **2015**, *3*, 424–430.

(5) Li, J.; Yan, J.; Wen, D.; Khan, W. U.; Shi, J.; Wu, M.; Su, Q.; Tanner, P. A. Advanced Red Phosphors for White Light-Emitting Diodes. *J. Mater. Chem. C* **2016**, *4*, 8611–8623.

(6) McKittrick, Joanna and Shea-Rohwer, Lauren E., Review: Down Conversion Materials for Solid-State Lighting. *J. Am. Ceram. Soc.* **2014**, *97*, 1327–1352.

(7) Ignatovych, M.; Fasoli, M.; Kelemen, A. Thermoluminescence Study of Cu, Ag and Mn Doped Lithium Tetraborate Single Crystals and Glasses. *Radiat. Phys. Chem.* **2012**, *81*, 1528 – 1532.

(8) Chen, Q.; Wu, J.; Ou, X.; Huang, B.; Almutlaq, J.; Zhumekenov, A. A.; Guan, X.; Han, S.; Liang, L.; Yi, Z. et al. All-Inorganic Perovskite Nanocrystal Scintillators. *Nature* **2018**, *561*, 88–93.

(9) Zhydachevskii, Y.; Galanciak, D.; Kobyakov, S.; Berkowski, M.; Kamińska, A.; Suchocki, A.; Zakharko, Y.; Durygin, A. Photoluminescence Studies of Mn 4+ Ions in YAlO 3 Crystals at Ambient and High Pressure. *J. Phys.: Condens. Matter* **2006**, *18*, 11385.

(10) Qin, X.; Liu, X.; Huang, W.; Bettinelli, M.; Liu, X. Lanthanide-Activated Phosphors Based on 4f-5d Optical Transitions: Theoretical and Experimental Aspects. *Chem. Rev.* **2017**, *117*, 4488–4527.

(11) Schweizer, S.; Hobbs, L. W.; Secu, M.; Spaeth, J.-M.; Edgar, A.; Williams, G. V. M. Photostimulated Luminescence in Eu-Doped Fluorochlorozirconate Glass Ceramics. *Appl. Phys. Lett.* **2003**, *83*, 449–451.

(12) Setlur, A. A.; Lyons, R. J.; Murphy, J. E.; Prasanth Kumar, N.; Satya Kishore, M. Blue Light-Emitting Diode Phosphors Based upon Oxide, Oxyhalide, and Halide Hosts. *ECS J. Solid State Sci.Tech.* **2013**, *2*, R3059–R3070.

(13) Birowosuto, M. D.; Dorenbos, P. Novel γ- and X-Ray Scintillator Research: On the Emission Wavelength, Light Yield and Time Response of Ce3+ Doped Halide

Scintillators. *Phys. Status Solidi* **2007**, *206*, 9–20.

(14) Geusic, J. E.; Marcos, H. M.; Van Uitert, L. G. Laser Oscillators in Nd-Doped Yttrium Aluminum, Tyyrium Gallium and Gadolinium Garnets. *Appl. Phys. Lett.* **1964**, *4*, 182–184.

(15) Heikenfeld, J.; Garter, M.; Lee, D. S.; Birkhahn, R.; Steckl, A. J. Red Light Emission by Photoluminescence and Electroluminescence from Eu-Doped GaN. *Appl. Phys. Lett.* **1999**, *75*, 1189–1191.

(16) Wang, X.-J.; Jia, D.; Yen, W. Mn^{2+} Activated Green, Yellow, and Red Long Persistent Phosphors. *J. Lumin.* **2003**, *102-103*, 34 – 37.

(17) Zhydachevskii, Y.; Durygin, A.; Suchocki, A.; Matkovskii, A.; Sugak, D.; Bilski, P.; Warchol, S. Mn-Doped YAlO3 Crystal: A New Potential TLD Phosphor. *Nucl Instrum Methods Phys Res B* **2005**, *227*, 545 – 550.

(18) Kim, J. S.; Jeon, P. E.; Choi, J. C.; Park, H. L.; Mho, S. I.; Kim, G. C. Warm-White-Light Emitting Diode Utilizing a Single-Phase Full-Color $Ba_3MgSi_2O_8$:Eu^{2+}, Mn^{2+} Phosphor. *Appl. Phys. Lett.* **2004**, *84*, 2931–2933.

(19) Bhargava, R. Doped Nanocrystalline Materials - Physics and Applications. *J. Lumin.* **1996**, *70*, 85 – 94.

(20) Morell, A.; El Khiati, N. Green Phosphors for Large Plasma TV Screens. *J Electrochem Soc.* **1993**, *140*, 2019–2022.

(21) Xu, Y. K.; Adachi, S. Properties of Na_2SiF_6:Mn^{4+} and Na_2GeF_6:Mn^{4+} Red Phosphors Synthesized by Wet Chemical Etching. *J Appl. Phys.* **2009**, *105*, 013525.

(22) Soo, Y. L.; Ming, Z. H.; Huang, S. W.; Kao, Y. H.; Bhargava, R. N.; Gallagher, D. Local Structures Around Mn Luminescent Centers in Mn-Doped Nanocrystals of ZnS. *Phys. Rev. B* **1994**, *50*, 7602–7607.

(23) Brik, M. G.; Srivastava, A. M. on the Optical Properties of the Mn^{+4} Ion in Solids. *J. Lumin.* **2013**, *133*, 69–72.

(24) Brik, M.; Srivastava, A. Comparative Crystal Field Analysis of Energy Level Schemes and Nephelauxetic Effect for Cr^{4+}, Cr^{3+}, and Mn^{4+} Ions in $Y_2Sn_2O_7$ Pyrochlore. *Opt. Mater.* **2013**, *35*, 1251 – 1256.

(25) Smith, T.; Guild, J. the C.I.E. Colorimetric Standards and Their Use. *Trans. Opt. Soc.* **1931**, *33*, 73–134.

(26) McMorran, B. J.; Agrawal, A.; Anderson, I. M.; Herzing, A. A.; Lezec, H. J.; McClelland, J. J.; Unguris, J. Electron Vortex Beams with High Quanta of Orbital Angular Momentum. *Science* **2011**, *331*, 192–195.

(27) Negi, D. S.; Idrobo, J. C.; Rusz, J. Probing the Localization of Magnetic Dichroism by Atomic-Size Astigmatic and Vortex Electron Beams. *Sci. Rep.* **2018**, *8*, 4019.

(28) Heyd, J.; Scuseria, G. E.; Ernzerhof, M. Hybrid Functionals Based on a Screened Coulomb Potential. *The J. Chem. Phys.* **2003**, *118*, 8207.

(29) Anisimov, V. I.; Zaanen, J.; Andersen, O. K. Band Theory and Mott Insulators: Hubbard U Instead of Stoner I. *Phys. Rev. B* **1991**, *44*, 943–954.

(30) Anisimov, V. I.; Aryasetiawan, F.; Lichtenstein, A. I. First-Principles Calculations of the Electronic Structure and Spectra of Strongly Correlated Systems: The LDa + U Method. *J. Phys.: Condens. Matter* **1997**, *9*, 767–808.

(31) Hedin, L. New Method for Calculating the One-Particle Green's Function with Application to the Electron-Gas Problem. *Phys. Rev.* **1965**, *139*, A796.

(32) Hedin, L.; Lundqvist, S. Effects of Electron-Electron and Electron-Phonon Interactions on the One-Electron States of Solids. *Solid State Phys.* **1970**, *23*, 1–181.

(33) Salpeter, E. E.; Bethe, H. A. a Relativistic Equation for Bound-State Problems. *Phys. Rev.* **1951**, *84*, 1232–1242.

(34) Bockstedte, M.; Marini, A.; Pankratov, O.; Rubio, A. Many-Body Effects in the Excitation Spectrum of a Defect in SiC. *Phys. Rev. Lett.* **2010**, *105*, 026401.

(35) Surh, M. P.; Chacham, H.; Louie, S. G. Quasiparticle Excitation Energies for the E-Center Defect in LiCl. *Phys. Rev. B* **1995**, *51*, 7464.

(36) Ma, Y.; Rohlfing, M. Optical Excitation of Deep Defect Levels in Insulators Within Many-Body Perturbation Theory: The F Center in Calcium Fluoride. *Phys. Rev. B - Condens. Matter Mater. Phys* **2008**, *77*, 115118.

(37) Onida, G.; Nazionale, I.; Vergata, R. T.; Scientifica, R.; Roma, I. Electronic Excitations : Density-Functional Versus Many-Body Green's-Function Approaches. *Rev. Mod. Phys.* **2002**, *74*, 601.

(38) Di Valentin, C., Botti, S., Cococcioni, M., Eds. *First Principles Approaches to Spectroscopic Properties of Complex Materials*; Springer Berlin Heidelberg: Berlin, Heidelberg, 2014.

(39) Körbel, S.; Kammerlander, D.; Sarmiento-Pérez, R.; Attaccalite, C.; Marques, M. A. L.; Botti, S. Optical Properties of Cu-Chalcogenide Photovoltaic Absorbers from Self-Consistent *GW* and the Bethe-Salpeter Equation. *Phys. Rev. B* **2015**, *91*, 075134.

(40) Botti, S.; Kammerlander, D.; Marques, M. A. L. Band Structures of Cu_2ZnSnS_4 and $Cu_2ZnSnSe_4$ from Many-Body Methods. *Appl. Phys. Lett.* **2011**, *98*, 241915.

(41) Vinson, J.; Rehr, J. J. Ab Initio Bethe-Salpeter Calculations of the X-Ray Absorption Spectra of Transition Metals at the *L*-Shell Edges. *Phys. Rev. B* **2012**, *86*, 195135.

(42) Rinke, P.; Janotti, A.; Scheffler, M.; Van de Walle, C. G. Defect Formation Energies Without the Band-Gap Problem: Combining Density-Functional Theory and the *GW* Approach for the Silicon Self-Interstitial. *Phys. Rev. Lett.* **2009**, *102*, 026402.

(43) Chen, W.; Pasquarello, A. Correspondence of Defect Energy Levels in Hybrid Density Functional Theory and Many-Body Perturbation Theory. *Phys. Rev. B* **2013**, *88*, 115104.

(44) Lewis, D. K.; Matsubara, M.; Bellotti, E.; Sharifzadeh, S. Quasiparticle and Hybrid Density Functional Methods in Defect Studies: An Application to the Nitrogen Vacancy in GaN. *Phys. Rev. B* **2017**, *96*, 235203.

(45) Carter, D. J.; Fuchs, M.; Stampfl, C. Vacancies in GaN Bulk and Nanowires: Effect of Self-Interaction Corrections. *J. Phys.: Condens Matter* **2012**, *24*, 255801.

(46) Gomes, L. C.; Trevisanutto, P. E.; Carvalho, A.; Rodin, A. S.; Castro Neto, A. H. Strongly Bound Mott-Wannier Excitons in GeS and GeSe Monolayers. *Phys. Rev. B* **2016**, *94*, 155428.

(47) Qiu, D. Y.; da Jornada, F. H.; Louie, S. G. Environmental Screening Effects in 2D Materials: Renormalization of the Bandgap, Electronic Structure, and Optical Spectra of Few-Layer

Black Phosphorus. *Nano Letters* **2017**, *17*, 4706–4712.

(48) Malashevich, A.; Jain, M.; Louie, S. G. First-Principles DFT + *GW* Study of Oxygen Vacancies in Rutile TiO_2. *Phys. Rev. B* **2014**, *89*, 075205.

(49) Lany, S.; Zunger, A. Many-Body *GW* Calculation of the Oxygen Vacancy in ZnO. *Phys. Rev. B* **2010**, *81*, 113201.

(50) Qiu, D. Y.; da Jornada, F. H.; Louie, S. G. Optical Spectrum of MoS_2: Many-Body Effects and Diversity of Exciton States. *Phys. Rev. Lett.* **2013**, *111*, 216805.

(51) Shi, H.; Pan, H.; Zhang, Y. W.; Yakobson, B. I. Quasiparticle Band Structures and Optical Properties of Strained Monolayer MoS_2 and WS_2. *Phys. Rev. B - Condens. Matter Mater. Phys* **2013**, *87*, 155304.

(52) Azhikodan, D.; Nautiyal, T.; Shallcross, S.; Sharma, S. an Anomalous Interlayer Exciton in MoS2. *Sci. Rep.* **2016**, *6*.

(53) Qiu, D. Y.; da Jornada, F. H.; Louie, S. G. Screening and Many-Body Effects in Two-Dimensional Crystals: Monolayer MoS_2. *Phys. Rev. B* **2016**, *93*, 235435.

(54) He, J.; Chen, M. X.; Chen, X. Q.; Franchini, C. Structural Transitions and Transport-Half-Metallic Ferromagnetism in $LaMnO_3$ at Elevated Pressure. *Phys. Rev. B - Condens. Matter Mater. Phys* **2012**, *85*, 195135.

(55) Xu, L.; Yang, M.; Wang, S. J.; Feng, Y. P. Electronic and Optical Properties of the Monolayer Group-IV Monochalcogenides MX (M = Ge, Sn; X = S, Se, Te). *Phys. Rev. B* **2017**, *95*, 235434.

(56) Flores, M. A.; Menéndez-Proupin, E.; Orellana, W.; Huang, D.; Jiang, J.-W.; Guo, J. Defect Properties of Sn- and Ge-Doped ZnTe: Suitability for Intermediate-Band Solar Cells. *Semicond. Sci. Technol* **2018**, *33*.

(57) Jiang, H.; Gomez-Abal, R. I.; Rinke, P.; Scheffler, M. Localized and Itinerant States in Lanthanide Oxides United by *GW* @ LDA+U. *Phys. Rev. Lett.* **2009**, *102*, 126403.

(58) Jiang, H.; Gomez-Abal, R. I.; Rinke, P.; Scheffler, M. First-Principles Modeling of Localized *d* States with the *GW*@LDA+U Approach. *Phys. Rev. B* **2010**, *82*, 045108.

(59) Poteryaev, A. I.; Lichtenstein, A. I.; Kotliar, G. Nonlocal Coulomb Interactions and Metal-Insulator Transition in Ti2O3: A Cluster LDA+DMFT Approach. *Phys. Rev. Lett.* **2004**, *93*, 086401.

(60) Sarsari, I. A.; Pemmaraju, C. D.; Salamati, H.; Sanvito, S. Many-Body Quasiparticle Spectrum of Co-Doped ZnO: A *GW* Perspective. *Phys. Rev. B* **2013**, *87*, 245118.

(61) Lorke, M.; Frauenheim, T.; da Rosa, A. L. Many-Body Electronic Structure Calculations of Eu-Doped ZnO. *Phys. Rev. B* **2016**, *93*, 115132.

(62) Foulkes, W.; Mitas, L.; Needs, R.; Rajagopal, G. Quantum Monte Carlo Simulations of Solids. *Rev. Mod. Phys.* **2001**, *73*, 33–83.

(63) Needs, R. J.; Towler, M. D.; Drummond, N. D.; López Ríos, P. Continuum Variational and Diffusion Quantum Monte Carlo Calculations. *J. Phys.: Condensed Matter* **2010**, *22*, 023201.

(64) Shulenburger, L.; Mattsson, T. R. Quantum Monte Carlo Applied to Solids. *Phys. Rev. B - Condens. Matter Mater. Phys* **2013**, *88*, 245117.

(65) Kent, P. R. C.; Hood, R. Q.; Towler, M. D.; Needs, R. J.; Rajagopal, G. Quantum Monte Carlo Calculations of the One-Body Density Matrix and Excitation Energies of Silicon. *Phys. Rev. B* **1998**, *57*, 15293.

(66) Hood, R. Q.; Kent, P. R. C.; Needs, R. J.; Briddon, P. R. Quantum Monte Carlo Study of the Optical and Diffusive Properties of the Vacancy Defect in Diamond. *Phys. Rev. Lett.* **2003**, *91*, 076403.

(67) Drüppel, M.; Deilmann, T.; Krüger, P.; Rohlfing, M. Diversity of Trion States and Substrate Effects in the Optical Properties of an MoS2 Monolayer. *Nat. Commun.* **2017**, *8*, 2117.

(68) Patrick, C. E.; Giustino, F. Quantum Nuclear Dynamics in the Photophysics of Diamondoids. *Nat. Commun.* **2013**, *4*, 1–7.

(69) Mitra, C.; Krogel, J. T.; Santana, J. A.; Reboredo, F. A. Many-Body Ab Initio Diffusion Quantum Monte Carlo Applied to the Strongly Correlated Oxide NiO. *J. Chem. Phys.* **2015**, *143*, 164710–164705.

(70) Ma, F.; Zhang, S.; Krakauer, H. Excited State Calculations in Solids by Auxiliary-Field Quantum Monte Carlo. *New J. Phys.* **2013**, *15*.

(71) Santana, J. A.; Krogel, J. T.; Kim, J.; Kent, P. R. C.; Reboredo, F. A. Structural Stability and Defect Energetics of ZnO from Diffusion Quantum Monte Carlo. *J. Chem. Phys.* **2015**, *142*.

(72) Kolorenč, J.; Hu, S.; Mitas, L. Wave Functions for Quantum Monte Carlo Calculations in Solids: Orbitals from Density Functional Theory with Hybrid Exchange-Correlation Functionals. *Phys. Rev. B - Condens. Matter Mater. Phys* **2010**, *82*, 115108.

(73) Schiller, J. A.; Wagner, L. K.; Ertekin, E. Phase Stability and Properties of Manganese Oxide Polymorphs: Assessment and Insights from Diffusion Monte Carlo. *Phys. Rev. B - Condens. Matter Mater. Phys* **2015**, *92*, 235209.

(74) Saritas, K.; Krogel, J. T.; Kent, P. R. C.; Reboredo, F. A. Diffusion Monte Carlo: A Pathway Towards an Accurate Theoretical Description of Manganese Oxides. *Phys. Rev. Materials* **2018**, *2*, 085801.

(75) Saritas, K.; Krogel, J. T.; Reboredo, F. A. Relative Energies and Electronic Structures of CoO Polymorphs Through Ab Initio Diffusion Quantum Monte Carlo. *Phys. Rev. B* **2018**, *98*, 155130.

(76) Leung, W.-K.; Needs, R. J.; Rajagopal, G.; Itoh, S.; Ihara, S. Calculations of Silicon Self-Interstitial Defects. *Phys. Rev. Lett.* **1999**, *83*, 2351–2354.

(77) Alfè, D.; Gillan, M. J. Schottky Defect Formation Energy in MgO Calculated by Diffusion Monte Carlo. *Phys. Rev. B - Condens. Matter Mater. Phys* **2005**, *71*, 220101.

(78) Yu, J.; Wagner, L. K.; Ertekin, E. Fixed-Node Diffusion Monte Carlo Description of Nitrogen Defects in Zinc Oxide. *Phys. Rev. B* **2017**, *95*, 075209.

(79) Santana, J. A.; Mishra, R.; Krogel, J. T.; Borisevich, A. Y.; Kent, P. R.; Pantelides, S. T.; Reboredo, F. A. Quantum Many-Body Effects in Defective Transition-Metal-Oxide Superlattices. *J. Chem. Theory Comput.* **2017**, *13*, 5604–5609.

(80) Santana, J. A.; Krogel, J. T.; Kent, P. R. C.; Reboredo, F. A. Cohesive Energy and Structural Parameters of Binary Oxides of Groups IIa and IIIB from Diffusion Quantum Monte Carlo. *J. Chem. Phys.* **2016**, *144*, 174707.

(81) Zheng, H.; Wagner, L. K. Computation of the Correlated Metal-Insulator Transition in Vanadium Dioxide from First

Principles. *Phys. Rev. Lett.* **2015**, *114*, 176401.

(82) Kylänpää, I.; Balachandran, J.; Ganesh, P.; Heinonen, O.; Kent, P. R. C.; Krogel, J. T.; Materials, N.; Ridge, O.; Ridge, O. Accuracy of Ab Initio Electron Correlation and Electron Densities in Vanadium Dioxide. *Phys. Rev. Materials* **2017**, *1*, 065408.

(83) Shulenburger, L.; Baczewski, A. D.; Zhu, Z.; Guan, J.; Tománek, D. the Nature of the Interlayer Interaction in Bulk and Few-Layer Phosphorus. *Nano Lett.* **2015**, *15*, 8170–8175.

(84) Drummond, N. D.; Monserrat, B.; Lloyd-Williams, J. H.; Ríos, P. L.; Pickard, C. J.; Needs, R. J. Quantum Monte Carlo Study of the Phase Diagram of Solid Molecular Hydrogen at Extreme Pressures. *Nat. Commun.* **2015**, *6*, 1–6.

(85) Bartlett, R. J.; Musiał, M. Coupled-Cluster Theory in Quantum Chemistry. *Rev. Mod. Phys.* **2007**, *79*, 291–352.

(86) Čižek, J. On the Correlation Problem in Atomic and Molecular Systems. Calculation of Wavefunction Components in Ursell-Type Expansion Using Quantum-Field Theoretical Methods. *J Chem Phys* **1966**, *45*, 4256–4266.

(87) Saritas, K.; Grossman, J. C. Accurate Isomerization Enthalpy and Investigation of the Errors in Density Functional Theory for Dihydroazulene/Vinylheptafulvene Photochromism Using Diffusion Monte Carlo. *J Phys. Chem. C* **2017**, *121*, 26677–26685.

(88) Williamson, A. J.; Hood, R. Q.; Grossman, J. C. Linear-Scaling Quantum Monte Carlo Calculations. **2001**, *87*.

(89) Alfè, D.; Gillan, M. J. Linear-Scaling Quantum Monte Carlo Technique with Non-Orthogonal Localized Orbitals. *J. Phys.: Condens. Matter* **2004**, *16*, L305–L311.

(90) Reboredo, F. A.; Williamson, A. J. Optimized Nonorthogonal Localized Orbitals for Linear Scaling Quantum Monte Carlo Calculations. *Phys. Rev. B - Condens. Matter Mater. Phys* **2005**, *71*, 121105.

(91) Du, M. H. Chemical Trends of Mn^{4+} Emission in Solids. *J. Mater. Chem. C* **2014**, *2*, 2475–2481.

(92) Bernu, B.; Ceperley, D. M. the Calculation of Excited State Properties with Quantum Monte Carlo. *J. Chem. Phys.* **1988**, *89*, 6316.

(93) Needs, R. J.; Kent, P. R. C.; Porter, A. R.; Towler, M. D.; Rajagopal, G. Quantum Monte Carlo Calculations for Ground and Excited States. *InterNatl. J. (Wash.) of Quantum Chemistry* **2002**, *86*, 218–225.

(94) Williamson, A. J.; Hood, R. Q.; Needs, R. J.; Rajagopal, G. Diffusion Quantum Monte Carlo Calculations of the Excited States of Silicon. *Phys. Rev. B* **1998**, *57*, 12140.

(95) Mostaani, E.; Szyniszewski, M.; Price, C. H.; Maezono, R.; Danovich, M.; Hunt, R. J.; Drummond, N. D.; Falko, V. I. Diffusion Quantum Monte Carlo Study of Excitonic Complexes in Two-Dimensional Transition-Metal Dichalcogenides. *Phys. Rev. B* **2017**, *96*, 075431.

(96) Williamson, A. J.; Grossman, J. C.; Hood, R. Q.; Puzder, A.; Galli, G. Quantum Monte Carlo Calculations of Nanostructure Optical Gaps: Application to Silicon Quantum Dots. *Phys. Rev. Lett.* **2002**, *89*, 196803.

(97) Puzder, A.; Williamson, A. J.; Reboredo, F. A.; Galli, G. Structural Stability and Optical Properties of Nanomaterials with Reconstructed Surfaces. *Phys. Rev. Lett.* **2003**, *91*, 157405.

(98) Hsing, C. R.; Wei, C. M.; Drummond, N. D.; Needs, R. J. Quantum

Monte Carlo Studies of Covalent and Metallic Clusters: Accuracy of Density Functional Approximations. *Phys. Rev. B - Condens. Matter Mater. Phys* **2009**, *79*, 245401.

(99) Geschwind, S.; Kisliuk, P.; Klein, M. P.; Remeika, J. P.; Wood, D. L. Sharp-Line Fluorescence, Electron Paramagnetic Resonance, and Thermoluminescence of Mn^{4+} in -Al2O3. *Phys. Rev.* **1962**, *126*, 1684–1686.

(100) Arai, T.; Adachi, S. Excited States of $3d^3$ Electrons in K_2SiF_6:Mn^{4+} Red Phosphor Studied by Photoluminescence Excitation Spectroscopy. *Japanese J. Appl. Phys.* **2011**, *50*, 092401.

(101) Dunphy, K.; Duley, W. W. Multiphoton Excitation of Mn^{4+} and Cr^{3+} Luminescence in MgO. *Phys. Chem. Solids* **1990**, *51*, 1077–1082.

(102) Perdew, J.; Burke, K.; Ernzerhof, M. Generalized Gradient Approximation Made Simple. *Phys. Rev. Lett.* **1996**, *77*, 3865–3868.

(103) E. Pavarini, F. A., E. Koch; Jarrell, M. *Correlated Electrons: From Models to Materials Modeling and Simulation*; Forschungszentrum Julich: Julich, Germany, 2012; Vol. 2.

(104) Santos, R.; Longhinotti, E.; Freire, V.; Reimberg, R.; Caetano, E. Elucidating the High-K Insulator Îś-Al2O3 Direct/indirect Energy Band Gap Type Through Density Functional Theory Computations. *Chem. Phys. Lett.* **2015**, *637*, 172 – 176.

(105) Choi, M.; Janotti, A.; Van de Walle, C. G. Native Point Defects and Dangling Bonds in α-Al2O3. *J Appl. Phys.* **2013**, *113*, 044501.

(106) Ealet, B.; Elyakhloufi, M.; Gillet, E.; Ricci, M. Electronic and Crystallographic Structure of γ-Alumina Thin Films. *Thin Solid Films* **1994**, *250*, 92 – 100.

(107) Heo, S.; Cho, E.; Lee, H.-I.; Park, G. S.; Kang, H. J.; Nagatomi, T.; Choi, P.; Choi, B.-D. Band Gap and Defect States of MgO Thin Films Investigated Using Reflection Electron Energy Loss Spectroscopy. *AIP Adv.* **2015**, *5*, 077167.

(108) Shi, L.-B.; Liu, X.-Y.; Dong, H.-K. Investigation of the Interface Characteristics of Y_2O_3/GaAs Under Biaxial Strain, Triaxial Strain, and Non-Strain Conditions. *J Appl. Phys* **2016**, *120*, 105306.

(109) Zhang, S.; Xiao, R. Yttrium Oxide Films Prepared by Pulsed Laser Deposition. *J Appl. Phys* **1998**, *83*, 3842–3848.

(110) Brik, M. G.; Srivastava, A. M. Ab Initio Studies of the Structural, Electronic, and Optical Properties of K_2SiF_6 Single Crystals at Ambient and Elevated Hydrostatic Pressure. *J Electrochem Soc.* **2012**, *159*, J212–J216.

(111) Takahashi, T.; Adachi, S. Mn+4 Activated Red Photoluminescence in K_2SiF_6 Phosphor. *J Electrochem Soc.* **2008**, *155*, E183–E188.

(112) Medvedev, M. G.; Bushmarinov, I. S.; Sun, J.; Perdew, J. P.; Lyssenko, K. A. Density Functional Theory Is Straying from the Path Toward the Exact Functional. *Science* **2017**, *355*, 49–52.

(113) Du, M. H. Mn^{4+} Emission in Pyrochlore Oxides. *J. Lumin.* **2015**, *157*, 69–73.

(114) Kresse, G.; Furthmüller, J. Efficient Iterative Schemes for Ab Initio Total-Energy Calculations Using a Plane-Wave Basis Set. *Phys. Rev.. B, Condensed matter* **1996**, *54*, 11169–11186.

(115) Kresse, G.; Furthmüller, J. Efficiency of Ab-Initio Total Energy Calculations for Metals and Semiconductors Using a Plane-Wave Basis Set. *Computational Mater. Sci.* **1996**, *6*, 15–50.

(116) Kresse, G.; Joubert, D. from Ultrasoft Pseudopotentials to the Projector Augmented-Wave Method. *Phys. Rev. B* **1999**, *59*, 1758.

(117) Krogel, J. T. Nexus: A Modular Workflow Management System for Quantum Simulation Codes. *Comput. Phys. Commun.* **2016**, *198*, 154 – 168.

(118) Giannozzi, P.; Baroni, S.; Bonini, N.; Calandra, M.; Car, R.; Cavazzoni, C.; Ceresoli, D.; Chiarotti, G. L.; Cococcioni, M.; Dabo, I. et al. QUANTUM ESPRESSO: A Modular and Open-Source Software Project for Quantum Simulations of Materials. *J. Phys. Condens. Matter* **2009**, *21*, 395502.

(119) Perdew, J. P.; Zunger, A. Self-Interaction Correction to Density-Functional Approximations for Many-Electron Systems. *Phys. Rev. B* **1981**, *23*, 5048–5079.

(120) Dudarev, S. L.; Botton, G. A.; Savrasov, S. Y.; Humphreys, C. J.; Sutton, A. P. Electron-Energy-Loss Spectra and the Structural Stability of Nickel Oxide: An LSDA+U Study. *Phys. Rev. B* **1998**, *57*, 1505–1509.

(121) Drummond, N. D.; Towler, M. D.; Needs, R. J. Jastrow Correlation Factor for Atoms, Molecules, and Solids. *Phys. Rev. B - Condens. Matter Mater. Phys.* **2004**, *70*, 235119.

(122) Umrigar, C. J.; Filippi, C. Energy and Variance Optimization of Many-Body Wave Functions. *Phys. Rev. Lett.* **2005**, *94*, 150201.

(123) Krogel, J. T.; Santana, J. A.; Reboredo, F. A. Pseudopotentials for Quantum Monte Carlo Studies of Transition Metal Oxides. *Phys. Rev. B* **2016**, *93*, 075143.

(124) Fuchs, M.; Scheffler, M. Ab Initio Pseudopotentials for Electronic Structure Calculations of Poly-Atomic Systems Using Density-Functional Theory. *Comput. Phys. Commun.* **1999**, *119*, 67–98.

(125) Benali, A.; Shulenburger, L.; Krogel, J. T.; Zhong, X.; Kent, P. R. C.; Heinonen, O. Quantum Monte Carlo Analysis of a Charge Ordered Insulating Antiferromagnet: The Ti_4O_7 Magnéli Phase. *Phys. Chem. Chem. Phys.* **2016**, *18*, 1–12.

(126) Luo, Y.; Benali, A.; Shulenburger, L.; Krogel, J. T.; Heinonen, O.; Kent, P. R. C. Phase Stability of TiO_2 Polymorphs from Diffusion Quantum Monte Carlo. *New J. Phys.* **2016**, *18*, 113049.

(127) Saritas, K.; Mueller, T.; Wagner, L.; Grossman, J. C. Investigation of a Quantum Monte Carlo Protocol to Achieve High Accuracy and High-Throughput Materials Formation Energies. *J. Chem. Theory Comput.* **2017**, *13*, 1943–1951.